Controlling Nanotube Dimensions: Correlation between Composition, Diameter, and Internal Energy of Single-Walled Mixed Oxide Nanotubes

Suchitra Konduri, Sanjoy Mukherjee, and Sankar Nair*

School of Chemical & Biomolecular Engineering, Georgia Institute of Technology, 311 Ferst Drive NW, Atlanta, Georgia 30332-0100

ABSTRACT Control over the diameter of nanotubes is of significance in manipulating their properties, which depend on their dimensions in addition to their structure and composition. This aspect has remained a challenge in both carbon and inorganic nanotubes, since there is no obvious aspect of the formation mechanism that allows facile control over nanotube curvature. Here we develop and analyze a quantitative correlation between the composition, diameter, and internal energy of a class of single-walled mixed oxide aluminosilicogermanate (AlSiGeOH) nanotubes. A series of synthetic AlSiGeOH nanotubes with varying Si/Ge ratio are characterized by X-ray photoelectron spectroscopy, vibrational spectroscopy, energy dispersive X-ray spectroscopy, and X-ray diffraction to relate their compositions and diameters. We then study these nanotubes computationally by first parametrizing and validating a suitable interatomic potential model, and then using this potential model to investigate the internal energy of the nanotube as a function of diameter and composition *via* molecular dynamics simulations. There are minima in the internal energy as a function of diameter which progressively shift to larger nanotube diameters with increasing Ge content. An approximate analytical theory of nanotube diameter control, which contains a small number of physically significant fitted parameters, well describes the computational data by relating the composition and geometry to the strain energy of bending into a nanotube. The predicted composition-dependent shift in the energetically favored diameter follows the experimental trends. We suggest related methods of controlling nanotube energetics and their role in engineering nanotubes of controlled dimensions by liquid-phase chemistry.

KEYWORDS: nanotubes · diameter · composition · energy · molecular dynamics

Nanotubes have attracted significant attention over the past decade due to their remarkable physical properties, which allow their application as building blocks for a variety of nanostructured assemblies including high-strength nanocomposites, field-emitting surfaces, sensors, nanotransistors, electrode materials, and energy storage devices.[1–9] The exceptional properties of nanotubes are attributed to the combined effects of their nanoscale dimensions, hollow cylindrical shape, composition, structure, and porosity. Although there have been significant advances in characterizing the properties of nanotubes in relation to their structure, synthesis of nanotubes with well-controlled dimensions to achieve desired properties remains a challenging issue. This situation can be attributed to several factors, including challenges in understanding of the mechanism of nanotube synthesis and fast formation kinetics that impede mechanistic studies toward rational control of diameter. Additionally, there is an important conceptual difficulty, *i.e.*, the fact that the internal energy of carbon nanotubes (and other structurally analogous nanotube materials) decreases monotonically with increasing diameter.[6,10–14] Inorganic metal oxide nanotubes[15] are a more recently emerging class of nanomaterials that can be synthesized with tunable compositions *via* low-temperature liquid-phase chemistry. Such materials are attractive because of the vast range of technologically relevant properties afforded by metal oxides and because of the possibilities for more precise control over their dimensions, compositions, and resulting properties through relatively mild liquid-phase chemistry. Concepts relevant to nanotube diameter control (through control of interatomic bond energies and compositions on the inner and outer walls of the nanotube) appear to have been first speculated upon by Pauling[16] in the context of naturally occurring chrysotile nanotubes. However, synthetic model systems for testing and developing these concepts have remained elusive to the present day, with one notable exception as described below.

Here, we investigate a class of metal oxide aluminosilicogermanate (AlSiGeOH) nanotubes[17–19] that are synthetic analogues of the naturally occurring aluminosilicate nanotube mineral, imogolite. The cylindrical wall of these nanotubes can be visualized as a rolled-up sheet of gibbsite

*Address correspondence to sankar.nair@chbe.gatech.edu.

Received for review July 17, 2007 and accepted November 09, 2007.

Published online December 8, 2007.
10.1021/nn700104e CCC: $37.00

(aluminum hydroxide), with isolated silanol (≡Si—OH) or germanol (≡Ge—OH) groups linked to the inner surface of the nanotube wall. The nanotube wall is structurally ordered and is composed of an aluminum octahedron (AlO_6) with three oxygen atoms shared by silicon (SiO_4) or germanium (GeO_4) tetrahedra, while the other three oxygen atoms are shared with other Al octahedra in the nanotube wall. The nanotubes have an axial repeat unit of 0.85 nm, while the outer diameter of the nanotubes varies with relative composition of Si or Ge atoms in the structure. The general empirical formula of the unit cell is $(OH)_3Al_2O_3Si_xGe_{1-x}OH$, $0 \leq x \leq 1$. The energetics of the aluminosilicate end-member (*i.e.*, $x = 1$) nanotube has been examined in two previous computational studies, exploiting the availability of interatomic potentials for sheet-like (layered) aluminosilicate materials. An internal energy minimum was observed as a function of increasing nanotube diameter,[20,21] a phenomenon that is not observed in the case of carbon nanotubes or their inorganic analogues wherein the internal energy declines monotonically with increasing diameter. We also modeled the total energy of the aluminosilicate nanotube on the basis of the harmonic bond strain energies of Al−O and Si−O bonds. The bond strain energy was found to decrease monotonically for Al−O bonds with increasing nanotube radius, while that of the Si−O increased. This suggested that the competition between the Si−O and Al−O bond energies, and the functionalization of the inner wall of the nanotube with silanol groups, are responsible for the observed strain energy minimum and quite possibly the experimentally well-known monodispersity in diameter of the synthetic aluminosilicate nanotube. Such a possibility is also supported by recent advances[17] in understanding the mechanism of formation of such nanotubes, which involves the initial condensation of amorphous nanoparticles from dissolved precursors followed by slow transformation of the amorphous particles into short (~20 nm) nanotubes.

The objectives of the present investigation are to determine whether there is a well-defined relationship between generalized AlSiGeOH nanotube diameter and internal energy, and to ascertain whether this relationship correlates with the composition of the nanotubes. The existence of such a correlation would clearly have conceptual and practical implications for the engineering of metal oxide nanotubes with controlled dimensions. We employ primarily X-ray diffraction (XRD), X-ray photoelectron spectroscopy (XPS), Fourier-transform infrared (FTIR) spectroscopy, and also energy-dispersive X-ray spectroscopy (EDX) as characterization tools to experimentally relate the diameter and composition of a series of AlSiGeOH nanotubes that were hydrothermally synthesized with $0 \leq x \leq 1$. To allow computational investigation of the properties of such nanotubes, we parametrized additional components of the force field previously used for studying the aluminosilicate end-member that allow us to investigate germanium-containing nanotubes. We perform this force field parametrization by achieving good predictions of the structures of Ge-containing materials, and we further validate the force field by comparing the experimental infrared (IR) spectra of the nanotubes with power spectra obtained from Fourier transformation of computed velocity autocorrelation functions (VACF). Next, we investigate the nanotube energetics to examine the energy minimum phenomenon *via* molecular dynamics (MD) simulations. Finally, we generalize our approximate analytical description of nanotube diameter control[20] to the entire class of nanotubes studied here and comment on the implications for dimensional control of nanotube materials.

RESULTS AND DISCUSSION

Determination of the Chemical Composition of AlSiGeOH Nanotubes. Following the synthesis and purification of a series of AlSiGeOH nanotubes with varying x values (see Methods section), the compositional parameter x was estimated analytically *via* XPS and FTIR elemental composition characterization techniques. This is important because the value of x in the initial synthesis composition cannot be *a priori* assumed to exist in the final product, depending upon the mechanism and yield of the nanotube material. The elemental composition of the nanotubes was obtained using XPS by performing multiplex scans on the deposited films at specified energy ranges, a procedure also known as "deconvolution scanning". The data from these scans were used to estimate the elemental composition of the materials by standard techniques. The experimental conditions of the XPS scans are described further in the Methods section. A limitation of XPS is that it analyzes only a small amount of material, typically within a few nanometers of the X-ray incidence surface. We therefore developed a quantitative FTIR-based method (discussed below) to determine the composition of the nanotube materials. The XPS and FTIR analyses were further confirmed by EDX analysis of the nanotube samples.

Figure 1 shows the FTIR spectra of purified and freeze-dried mixed metal oxide nanotubes at various values of x in the synthesis solution. The spectra evolve continuously with x in the 800–1100 cm^{-1} region that represents vibrations involving Si and Ge atoms, whereas the 400–700 cm^{-1} region remains essentially constant in shape and represents vibrations involving the Al atoms (see Methods and Supporting Information for further discussion). The IR absorption intensities were employed to obtain information on the material composition. According to the Beer–Lambert law, the intensity of any IR absorption peak is a function of the number concentration of the atoms involved in the vibrational mode that it represents.[22] However, composition estimation from solid-state IR intensities must be carefully performed to account for inherent peak broad-

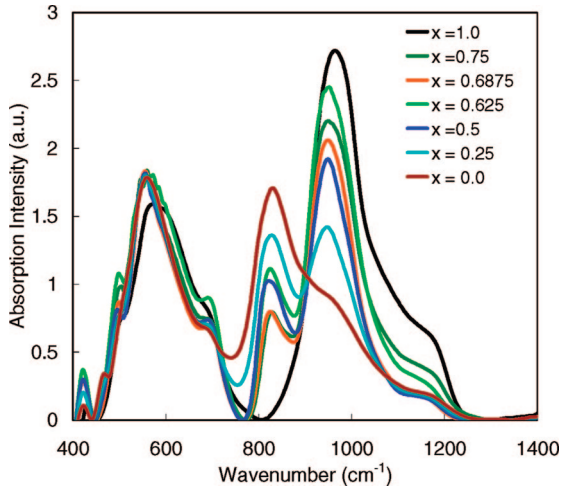

Figure 1. FTIR spectra of freeze-dried AlSiGeOH nanotubes produced from precursor solutions with $x = 1.0$ (black), 0.75 (dark green), 0.6875 (orange), 0.625 (light green), 0.5 (dark blue), 0.25 (light blue), and 0.0 (brown). The value of x is based on the composition of the synthesis solution.

ening effects.[23] This was achieved by deconvoluting each spectrum with a series of Gaussian peaks and relating integrated peak areas of appropriate peaks to the number concentration of the chosen vibrational mode and hence the composition of the material.[24] The Methods section and the Supporting Information give details of the procedures used. Figure 2 compares the results of FTIR, XPS, and EDX characterizations. The compositions obtained by the two techniques are in close agreement with each other and, in addition, follow the 45° line very closely, showing that the composition of the nanotubes in the synthesis product matches closely with the composition of the precursor solution. The result strongly suggests that the Si and Ge content in the nanotube can be readily controlled and reliably quantified. Since the nanotubes used in the present study were purified using dialysis, there are expected to be no residual precursors or other small-molecule impurities in the final nanotube products.

Force Field Parametrization and Validation. We have previously used the CLAYFF[25] force field for studying AlSiOH nanotubes, since this force field was well validated for a range of aluminosilicate layered minerals. To study the generalized class of AlSiGeOH nanotubes, we extended this force field to include tetrahedrally coordinated Ge atoms. In order to develop Ge parameters of good quality, we used the crystal structures of two known aluminogermanate materials with tetrahedrally coordinated Ge, namely the C-phase of $Na\{AlGeO_4\}$ and the D-phase of $K\{AlGeO_4\}$,[26] in addition to the structure of α-GeO_2[27] (which is analogous to α-quartz). The Methods section details the parametrization procedure, and Table 1 presents the final set of force field parameters. There is good agreement of the geometry-optimized lattice parameters and bond distances of tetrahedral Ge−O and Al−O bonds with the experimental structural details of the three materials (see Supporting Information), thus strongly suggesting that the force field describes their crystal structures well.

The quality of the Ge parametrization was further ascertained by comparing power spectra of AlSiGeOH nanotubes (calculated using geometry-optimized structures) with experimental FTIR spectra. Figure 3 shows the computed vibrational spectra and the corresponding experimental IR spectra for AlSiOH nanotubes, AlSiGeOH nanotubes with $x = 0.5$, and AlGeOH nanotubes, whereas the Supporting Information shows similar results for nanotubes with $x = 0.25$ and 0.75. Wada[28] previously assigned the vibrational modes observed in AlSiOH and AlGeOH nanotube materials into three groups: (i) frequencies between 400 and 700 cm^{-1} are due to Al−O−Al vibrations involving a large number of atoms (*i.e.*, phonon-like vibrations); (ii) higher frequency modes at ~930 and 975 cm^{-1} in AlSiOH nanotubes are due to localized vibrations in Si−OH and Al−O−Si linkages; and (iii) frequency modes at ~819 and 883 cm^{-1} in pure AlGeOH nanotubes are due to localized vibrations in Ge−OH and Al−O−Ge linkages. Analysis of our computed power spectra *via* deconvolution of each spectrum into a series of Gaussian peaks confirms these assignments (see Supporting Information). It should be noted that power spectra obtained from MD simulations can reliably reproduce only the positions of spectral bands observed in experimental vibrational spectrum. However, the intensities of the spectral bands cannot be compared directly between the computed power spectra and the experimental vibrational spectra because there is a large difference in the magnitude of atomic vibrations in MD simulations (that are ultimately reflected in the power spectrum) as compared to the fluctuations of the

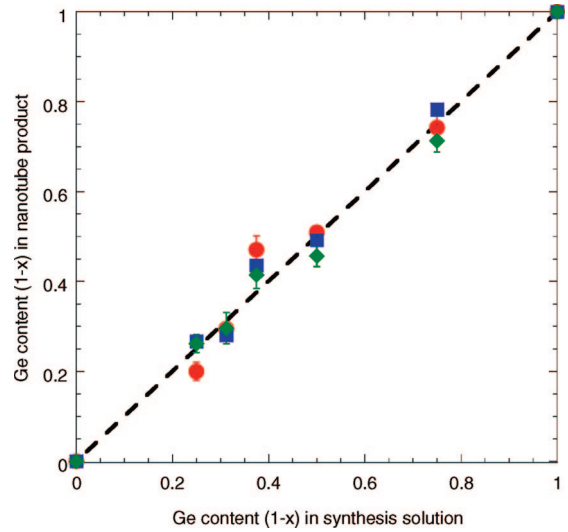

Figure 2. Comparison of the AlSiGeOH nanotube compositional analyses. Blue squares, red circles, and green diamonds indicate nanotube composition obtained using FTIR, XPS, and EDX techniques, respectively. The error bars on the XPS and EDX results were obtained by performing the elemental analysis in different sample areas.

TABLE 1. Force Field Parameters Used in MD Simulations for Calculating the Energetics of Single-Walled AlSiGeOH Nanotubes[a]

Nonbond Parameters for the Force Field

species	charge (e)	E (kcal/mol)	R_o (Å)
hydroxyl H	0.425		
hydroxyl O	−0.95	0.1554	3.5532
bridging oxygen between octahedral Al and tetrahedral Si or Ge	−1.05	0.1554	3.5532
octahedral Al	1.575	1.3298×10^{-6}	4.7943
tetrahedral Si	2.100	1.8405×10^{-6}	3.7064
tetrahedral Ge	2.100	1.8405×10^{-6}	4.7341

Bond Parameters for the Force Field

species i	species j	k (kcal/mol Å^2)	r_o (Å)
hydroxyl O	hydroxyl hydrogen	554.1349	1.000

[a]Parameters for Al, Si, O, and H are the same as in the original CLAYFF[25] force field, with additional parameters for Ge developed in this work using the same procedures as the CLAYFF.

corresponding electric dipole moments (which are ultimately reflected in experimental IR spectra).[25,29,30] The results shown in Figure 3 clearly suggest that the force field well reproduces the positions of the aforementioned absorption bands, although small deviations (~10 cm^{-1}) in the peak positions for Si−O and Ge−O vibrations are observed in the computed vibrational frequencies relative to the experimental vibrational spectra. This is a typical level of deviation in force fields developed for inorganic oxide materials.[25,30,31] In addition, the force field provides a very good prediction of the progressive shifts in the absorption band frequencies of Si−O and Ge−O vibrations with varying Ge content in the nanotubes. There are no significant differences between the nanotube materials in the calculated low-frequency (400–700 cm^{-1}) vibrational modes, as corroborated by experimental vibrational spectra. Overall, our validation studies support the applicability of the force field for the present investigation.

Correlation between Nanotube Composition, Diameter, and Energy. Molecular dynamics simulations were employed to calculate the total internal energy (potential and kinetic) per atom of the nanotubes as a function of x and the diameter (expressed in terms of the number of Al atoms, N, in the circumference of the nanotube). The Methods section presents details of the calculations. Figure 4 shows the baseline-subtracted energy (see following discussions) of the nanotubes on a per-atom basis *versus* the nanotube diameter for each composition investigated. It clearly indicates energy minima with respect to the diameter for each nanotube composition. Furthermore, the minima shift progressively to higher diameters with increasing Ge content. The minimum in the diameter-dependent energy of the AlSiOH end-member nanotube has been predicted independently with two different force fields[20,21] which differ only quantitatively in terms of the value of N at which the

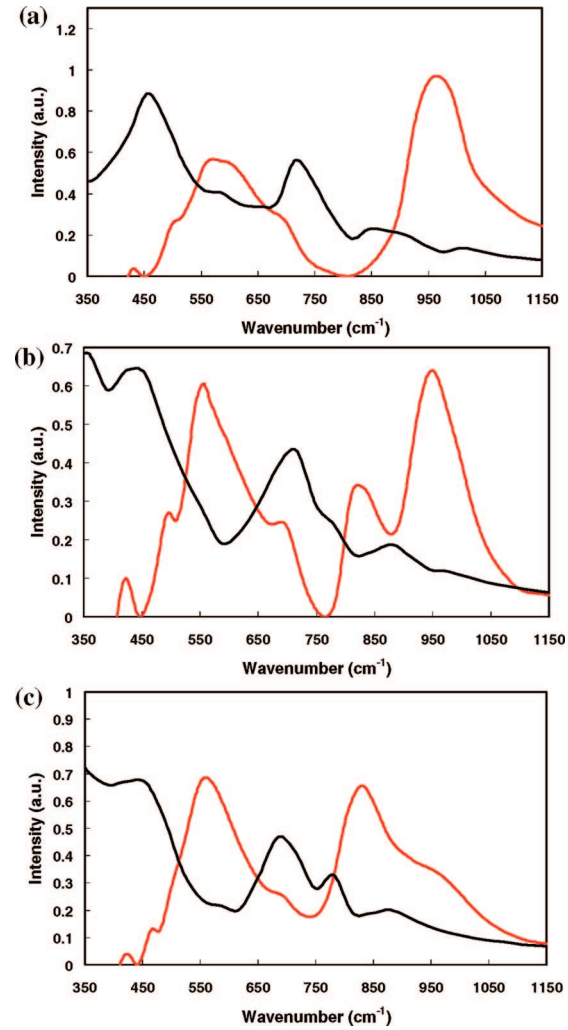

Figure 3. Comparison between computed vibrational power spectra (black) and experimental IR spectra (red) for (a) AlSiOH (x = 0), (b) AlSiGeOH (x = 0.5), and (c) AlGeOH (x = 1) nanotubes.

minimum occurs. Our earlier study[20] related the observed energy minimum in the AlSiOH nanotube to the difference in bond energies of Al−O and Si−O bond combined with material confinement into a cylindrical shape, to explain the monodispersity in diameter observed in single-walled AlSi nanotubes. In contrast, carbon nanotubes and their analogous materials do not exhibit such a behavior, and their energy was found to decrease monotonically with increasing nanotube diameter,[11] suggesting that internal energy criteria cannot be employed to synthesize carbon nanotubes with desired diameters. Figure 5 shows the computed radial breathing mode (RBM) frequency (f_{RBM}) of the nanotubes as a function of the radius (R). A power law dependence of the RBM frequency ($f_{RBM} = CR^{-1}$) on the nanotube radius is observed for all the nanotube compositions. The constant, C (cm^{-1} · nm), listed in Table 2, decreases with increasing Ge content. This is intuitive considering both the increased mass of Ge-containing nanotubes and the red shifts of stretching frequencies

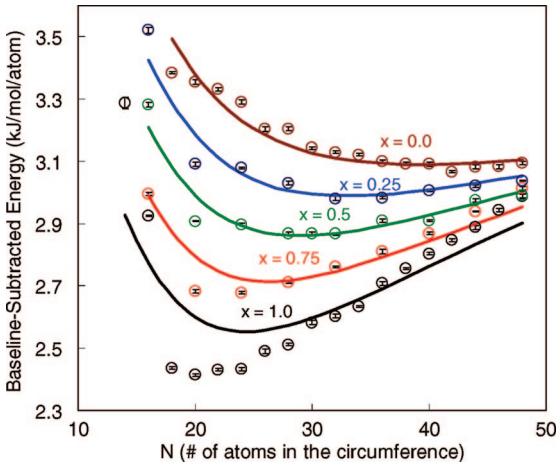

Figure 4. Total energy per atom at 298 K of AlSiGeOH nanotubes as a function of number of aluminum atoms (*N*) in the nanotube circumference for $x = 1$ (black), 0.75 (red), 0.5 (green), 0.25 (blue), and 0 (brown). Open symbols denote MD calculations, and solid lines denote harmonic strain energy model fits (see text).

observed in the IR spectra with increasing Ge content (*e.g.*, from ~930, 975 cm^{-1} for AlSiOH to 819, 883 cm^{-1} for AlGeOH). The power law dependence is also predicted by our model (described below).

Next, we extend our previously proposed "harmonic force constant" model[20] to include the strain energy contribution from Ge−O bonds. The model considers the nanotube as a cylindrical structure that is composed of "semi-rigid" aluminum octahedra and silicon/germanium tetrahedra, connected by oxygen atoms. The octahedra and tetrahedra are assumed to maintain their ideal O−Al−O, O−Si−O, and O−Ge−O bond angles (90°, 109.5°, and 109.5°, respectively) but allow stretching of their Al−O, Si−O, and Ge−O bonds. This idealization is in the spirit of the "central force" models[32,33] that describe structural changes in terms of bond length changes rather than bond angles. Such a model is primarily useful for predicting the total energy and related properties, not for accurate predictions of the geometry. Indeed, a further refined model of this type can be constructed by including bond angle distortions (in addition to bond lengths) as harmonic functions. Similarly, the MD simulations can be used to track the nanotube geometry (bond lengths and angles) as a function of diameter and composition.

TABLE 2. Comparison between Computed (from Normal-Mode Analysis) and Power Law Fits of the Theoretical Expression (Eq 4) for the RBM Frequency (Figure 5) in Different AlSiGeOH Nanotube Compositions[a]

composition (x)	computed power law	theoretical power law fit
1	$f_{RBM} = 47.5R^{-1.19}$	$48.6R^{-1.04}$
0.75	$f_{RBM} = 43.0R^{-1.10}$	$45.2R^{-1.04}$
0.5	$f_{RBM} = 41.0R^{-1.11}$	$42.0R^{-1.04}$
0.25	$f_{RBM} = 39.2R^{-1.14}$	$38.8R^{-1.04}$
0	$f_{RBM} = 35.5R^{-0.96}$	$35.7R^{-1.03}$

[a] R is the nanotube radius in nm, and the RBM frequencies are in cm^{-1}.

However, we believe that these extensions are currently unwarranted, because one cannot separate the energetic effects of bond angle and bond length changes using force fields based upon the Born ionic model (such as the present one). In particular, they contain a combination of many-body long-range terms as well as two-body short-range terms. Within our model, the strain energy contribution from the metal oxide bonds is given by harmonic bond stretching potentials,[20]

$$V_{Al\text{-}O} = K_1(d_1 - d_{1e})^2,\ V_{Si\text{-}O} = K_2(d_2 - d_{2e})^2,\ \text{and } V_{Ge\text{-}O} = K_3(d_3 - d_{3e})^2 \quad (1)$$

Here, K_1, K_2, and K_3 are the force constants, d_1, d_2, and d_3 are the bond lengths, and d_{1e}, d_{2e}, and d_{3e} are the equilibrium bond lengths of the Al−O, Si−O, and Ge−O bonds, respectively. The peripheral O−H bonds would make no contribution to the strain energy and are not considered. For a nanotube with N aluminum atoms in the circumference, there are $4N$ Al−O bonds, $3Nx$ Si−O bonds, $3N(1 - x)$ Ge−O bonds, and $14N$ atoms in the unit cell. The total internal energy of the nanotube is written as a summation of strain-independent and strain-dependent terms as given by eq 2:

$$E(N) = E_0 + 4NK_1(d_1 - d_{1e})^2 + 3N[xK_2(d_2 - d_{2e})^2 + (1 - x)K_3(d_3 - d_{3e})^2] \quad (2)$$

The strain-independent term (E_0) contains the kinetic energy and the remaining interatomic potential energies (*e.g.*, O−H) that do not depend on the nanotube radius but are still proportional to the number of atoms in the nanotube. Hence, we normalize the above equation by the total number of atoms in the unit cell:

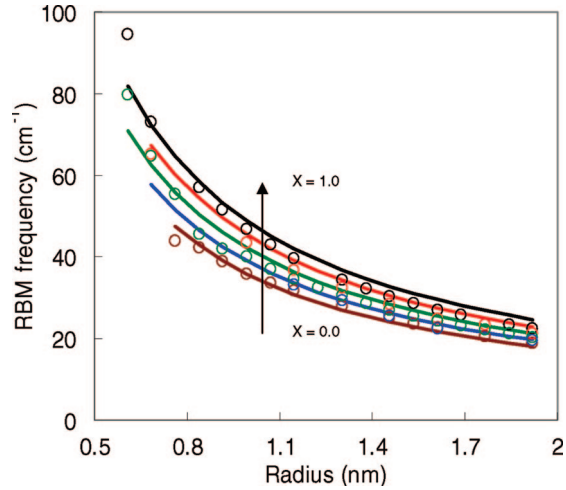

Figure 5. Computed radial breathing mode frequencies *versus* nanotube radius for AlSiGeOH nanotubes at $x = 1$ (black), 0.75 (red), 0.5 (green), 0.25 (blue), and 0 (brown). Open symbols denote MD simulations, and solid lines denote harmonic strain energy model fits (see text).

$$\bar{E}(N) = \bar{E}_0 + \frac{2}{7}K_1(d_1 - d_{1e})^2 + \frac{3}{14}[xK_2(d_2 - d_{2e})^2 + (1-x)K_3(d_3 - d_{3e})^2] \quad (3)$$

The bond lengths are a function of the number of atoms in the circumference and can be geometrically related to the nanotube radius as derived previously by us:[20] $d_1 = (2R/\sqrt{6})\sin(2\pi/N)$ and $d_2 = d_3 = d_1/\sqrt{2}$. An expression for the RBM frequency can be derived by considering the Lagrangian of the strain-dependent term in eq 2:

$$L = \frac{1}{2}m\dot{R}^2 - 4NK_1(d_1 - d_{1e})^2 - 3N[xK_2(d_2 - d_{2e})^2 + (1-x)K_3(d_3 - d_{3e})^2] \quad (4)$$

A Lagrangian equation, $d(\partial L/\partial \dot{R})/dt = \partial L/\partial R$, was then used to obtain the harmonic RBM frequency: $\omega_{RBM} = 2\pi f_{RBM} = \{4N(4K_1 + 1.5[xK_2 + (1-x)K_3])/3M\}^{1/2}\sin(2\pi/N)$. Here, the unit cell mass is $M = N(2m_{Al} + xm_{Si} + (1-x)m_{Ge} + 7m_O + 4m_H)$. The two expressions for $\bar{E}$ (eq 3) and f_{RBM} (eq 4) are then fitted simultaneously by nonlinear least-squares to the MD data (internal energies and RBM frequencies) to obtain the physical parameters: K_1, K_2, K_3, d_{1e}, d_{2e}, d_{3e}, and $\bar{E}_0$ (the latter parameter varies with the composition). The best fits for the equilibrium bond lengths are $d_{1e} = 0.197$ nm, $d_{2e} = 0.159$ nm, and $d_{3e} = 0.173$ nm. These are in accord with the nominal octahedral Al−O (~0.19 nm) and tetrahedral Si−O (~0.16 nm), Ge−O (~0.175 nm) bond lengths observed in oxide materials.[25,26,34,35] The fitted values for the harmonic force constants are $K_1 = 2.541 \times 10^4$ kJ mol^{-1} nm^{-2}, $K_2 = 5.849 \times 10^4$ kJ mol^{-1} nm^{-2}, and $K_3 = 1.567 \times 10^4$ kJ mol^{-1} nm^{-2}, respectively. These values suggest that the Ge−O bond has the weakest force constant, while the Al−O bond is intermediate between the Si−O and Ge−O bonds. The theoretical predictions yield power law fits of the RBM frequencies as a function of the radius, which are in very good agreement with the power law fits obtained from the MD simulations, as seen in Figure 5. The fitted values of the strain-independent baseline energy $\bar{E}_0$ are −571.26 kJ mol^{-1} ($x = 1$), −564.50 kJ mol^{-1} ($x = 0.75$), −557.69 kJ mol^{-1} ($x = 0.5$), −550.98 kJ mol^{-1} ($x = 0.25$), and −544.26 kJ mol^{-1} ($x = 0$). Considering that $\bar{E}_0$ is only a baseline energy parameter which is not correlated with the other parameters, the number of fitting parameters is quite small in relation to the quantity of data, as well as the internal constraints in the model which ensure convergence to physically realistic parameter values. For example, the RBM frequency depends only on a weighted summation of the three force constant parameters, which are therefore constrained since they must also be positive in sign. Additionally, the equilibrium bond distances and force constants are constrained further by the harmonic potential terms, which rapidly increase if these parameters assume unrealistic values.

The solid lines in Figure 4 show the predictions of the model with the final set of fitted parameters. The model well reproduces the progressive minima in the nanotube energy as a function of nanotube diameter and also predicts the internal energy *versus N* in close agreement with the computational data. While the contribution of Al−O bond strain energy to the total energy per atom of the nanotube decreases monotonically with increasing nanotube diameter, the Si−O bond strain energy increases,[20] and a similar increase in the Ge−O bond energy is also predicted by fitted parameters obtained in the present generalized model. These combined factors lead to an energy minimum in eq 3 at some intermediate value of *N*. Due to a larger Ge−O equilibrium bond length and weaker force constant in comparison to that of Si−O, the minimum shifts toward larger diameters as the Ge content increases. Thus, the incremental substitution of different tetrahedral metal atoms on the inner surface of a nanotube as a potential means of tuning the nanotube diameter indeed exhibits a strong correlation with the composition-dependent changes in the internal energy of the nanotube, as illustrated by the present case of Si/Ge substitution.

Comparison of Experimental and Predicted Nanotube Diameters. In order to quantitatively investigate whether the predicted continuous shift in outer diameter with composition occurs under real synthesis conditions, we considered two experimental techniques, namely X-ray diffraction (XRD) and transmission electron microscopy (TEM). The preparation of TEM samples wherein individual nanotubes (as opposed to nanotube bundles or overlapping nanotubes) can be imaged proved to be extremely challenging in general. In previous studies,[18,36] high-resolution images of individual AlSiOH and AlGeOH nanotubes could be obtained only with difficulty. Since the development of suitable TEM sample preparation and imaging methods was not the primary focus of this paper, we chose XRD as a more readily usable tool to estimate the outer diameter of the nanotubes. There is, however, an important factor to be considered regarding the use of XRD for this purpose. Unlike those of highly crystalline materials, the XRD patterns of nanotube bundles are not fully understood in a quantitative sense. Nanotube samples can have varying degrees of packing (ranging from two or three tubes in a bundle to many tubes packed in a solid-state arrangement). Previous investigators have interpreted XRD patterns of AlSiOH and AlGeOH nanotubes semiquantitatively in terms of either loosely packed or closely packed structures, resulting in somewhat different unit cell parameters.[18] However, it is now well-known from previous XRD simulation works on nanotube bundles[37–40] that the position (expressed as a *d*-spacing or a Bragg angle) of the intense low-angle

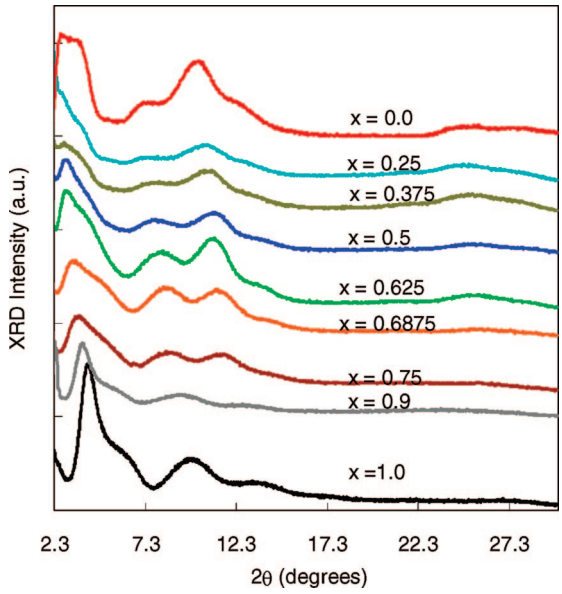

Figure 6. Grazing-angle X-ray diffraction patterns of AlSiGeOH nanotubes as a function of the compositional parameter *x*.

peak in the XRD pattern of a nanotube bundle is monotonically correlated to its diameter. Nanotubes of larger diameter scatter X-rays at lower Bragg angles. For our present purpose, we use this principle along with the previously determined outer diameters[18,36] of the end-member AlSiOH (2.2 nm) and AlGeOH (3.4 nm) nanotubes to estimate the outer diameters of synthesized AlSiGeOH nanotubes of intermediate composition on the basis of the measured positions of their low-angle XRD peaks. Figure 6 shows the XRD spectra of AlSiGeOH nanotubes with varying values of the compositional parameter *x*. A continuous shift of the first Bragg peak toward lower 2θ values can be observed with increasing Ge content. Assuming that the observed *d*-spacings for the two end-members differ from the known diameters of these two materials by a constant offset parameter, we calculate this offset and use it to determine the diameters of the nanotube materials of intermediate composition from the observed *d*-spacing.

Figure 7 compares the experimental estimates of nanotube diameter with the computational predictions and the predictions from the fitted strain energy model as a function of the composition. In the case of the computational and theoretical predictions, the nanotube whose diameter corresponds to the lowest internal energy is taken as the product expected in the synthesis carried out with that particular composition. The computational and model predictions match well, as might be expected considering that the physical parameters in the model were fitted using the computational data. Furthermore, they also correctly capture the experimentally observed trend in the diameter which increases with increasing Ge content. In other words, our current results clearly establish that there is a strong correlation between the composition, diameter, and internal energy of the AlSiGeOH nanotubes. The quantitative deviations of the experimentally estimated diameters from the computational and model predictions may be due to several factors. First, the relationship between the XRD peak position and the diameter is semiquantitative. Detailed modeling and fitting of the XRD patterns is required to obtain the diameter more accurately and is beyond the scope of this work. Second, the force field itself is fundamentally an approximation of the true energetics of the system. Finally, although the internal energy is almost always used to parametrize force fields and investigate the relative stability of similar materials, it is possible that a more accurate analysis would involve the calculation of quantities such as the free energy, as well as the consideration of the solution properties and mechanistic details of the synthesis. Although quantitative knowledge of the synthesis mechanism[17] is emerging, the above complications (*i.e.*, interpretation of experimental data, lack of accurate thermodynamic properties) are frequently encountered in the characterization and analysis of nanoscale materials. In our view, the present study shows for the first time a clear connection between nanotube dimensions, composition, and internal energy, thus substantiating the possibility of nanotube engineering *via* manipulation of interatomic potential energies and hence the thermodynamic properties.

In conclusion, it has been shown computationally, experimentally, and theoretically that the diameter of single-walled AlSiGeOH nanotubes can be controlled by liquid-phase synthesis involving different ratios of the tetrahedrally coordinated atoms (Si and Ge). Due to a difference in interatomic bond energies between the octrahedral (Al−O) and tetrahedral (Si−O and/or Ge−O) bonds on the outer and inner surfaces of the nanotube, respectively, a substantial energy minimum

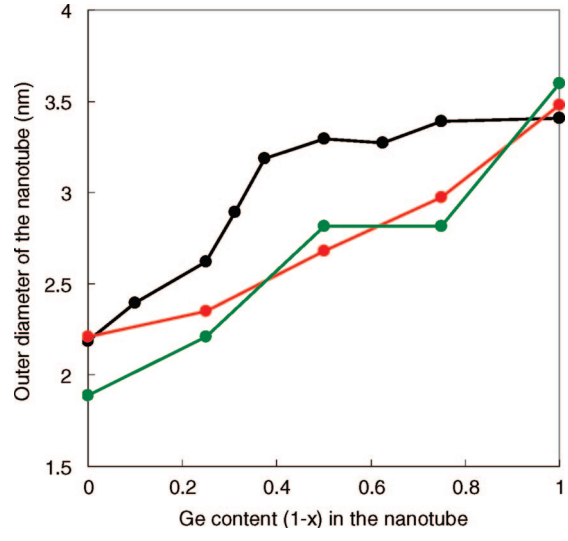

Figure 7. Comparison of AlSiGeOH nanotube diameters *versus* nanotube compositional parameter *x*: computed (green), theoretical (red), and experimental (black) results.

occurs with respect to the diameter. Furthermore, the energy minimum can be shifted to different diameters by changing the ratios of the two tetrahedrally coordinated elements (Si and Ge), as corroborated by the experimental results. Finally, the harmonic force constant model that relates the composition of the material to the nanotube energy can provide semiquantitative guidelines for tuning nanotube dimensions *via* appropriate selection of the octahedral/tetrahedral species combinations.

METHODS

Experimental Details. ***Nanotube Synthesis.*** Depending on the desired content of Ge in the mixed metal oxide nanotubes, tetraethylorthosilicate (TEOS, 99.99+% purity, Sigma-Aldrich) and tetraethylorthogermanate (TEOG, 99.99+%, Gelest) were added dropwise to a stirred solution of 5 mM $AlCl_3$ (99.99+%, Sigma-Aldrich) until the Al:(Si+Ge) ratio was 1.8, and then the mixture was left to stand for 45 min under vigorous stirring. A 0.1 N NaOH solution was then added at a rate of 0.3 mL/min until the pH of the solution reached 5.0. The pH was brought down immediately to 4.5 by dropwise addition of a solution containing 0.1 M HCl and 0.2 M acetic acid. The resulting clear solution was allowed to stir for 3 h and then reacted at 95 °C under reflux conditions for 120 h. The solution was then cooled to room temperature, and 0.1 N ammonia solution was added carefully until the pH reached 8.0. At this point, the suspension turned cloudy and was centrifuged at 3000 rpm for 20 min. The supernatant was discarded and the gel acidified with a few drops of 12 N HCl. The resulting solution was immediately dialyzed against deionized water for 120 h to remove any unreacted precursors as well as sodium and chloride ions. For XRD and XPS analysis, 5 mL of dialyzed solution was evaporated over a glass slide to deposit a film of nanotubes. These films were also used for EDX analysis. A portion of the dialyzed sample was freeze-dried into a powder for FTIR measurements.

Nanotube Characterization. Thin-film XRD analysis was performed on a PAnalytical X'pert Pro diffractometer operating with a Cu Kα source and equipped with a diffracted beam collimator and a Miniprop detector. The data were collected in grazing angle incidence mode, with the incident beam at a fixed grazing angle of 1° with respect to the sample plane and the detector scanning over angles from 2° to 30° with respect to the same plane. The nanotube films were analyzed for surface composition with a PH1 model SCA 1600 XPS instrument equipped with a monochromatic Al Kα source (1486.4 eV) and a spherical capacitor analyzer operating at 187.85 eV pass energy. High-resolution spectra (0.05 eV/step and 50 ms/step) were collected for peak deconvolution using Gauss−Lorentzian line shapes. EDX characterization of the Ge/Si ratio was carried out with an LEO 1550 scanninig electron microscope equipped with an energy-dispersive X-day detector, with an operating voltage of 5 kV. For each sample, at least three different locations (each of ~10 μm × 10 μm area) were scanned and the results averaged.

FTIR spectroscopy was performed on freeze-dried samples. The dialyzed liquid samples were immediately frozen at −20 °C before application of a vacuum. FTIR spectra were collected with a resolution of 8 cm^{-1} under vacuum conditions on a Bruker IFS 66v/S spectrometer. In order to provide a direct comparison between the IR spectra of AlSiGeOH nanotubes of different compositions, the spectra were normalized by Al composition in the nanotube, since the amount of Al in the chemical formula remains fixed. The absorption peaks from 400 to 790 cm^{-1} correspond to the Al−O vibrations.[19,28,41,42] Hence, all the IR spectra were normalized with respect to the integrated area in this frequency range. To quantify the relative amounts of Si and Ge, a rigorous curve-fitting procedure was developed that involved (i) fitting the IR spectra of pure AlSiOH and AlGeOH nanotubes accurately with Gaussian curves and (ii) fitting the IR spectra of mixed AlSiGeOH nanotubes by retaining the peak positions of Gaussian curves obtained from the previous step while varying their intensity and peak widths. From previous work,[28] it is known that the peak positions in the 800−1000 cm^{-1} range are of interest in the present compositional analysis. For AlGeOH nanotubes, absorption peaks due to Ge−O stretching vibrations are located within a range of ~819−883 cm^{-1}, while for AlSiOH nanotubes the absorption bands due to Si−O stretching vibrations are located within ~930−975 cm^{-1}. In AlSiGeOH nanotubes, the absorption peaks due to Si−O and Ge−O bonds coexist. The ratio of the areas of the respective peaks gives the ratio of Si and Ge in the nanotube product. See Supporting Information for further discussion of fitting procedures and analysis of results.

Computational Details. ***Force Field Parametrization.*** We employed the functional form of the recently developed CLAYFF force field[25] to describe the interactions between the atoms of the nanotube. The force field is based on the Born ionic model, with fractional charges assigned to each atom and Lennard-Jones (LJ) (12-6) potentials for Al−O, Si−O, Ge−O, and O−O interactions. The O−H bonds are described by a harmonic bond-stretching term:

$$E = \frac{e^2}{4\pi\epsilon_o}\sum_{i\neq j}\frac{q_i q_j}{r_{ij}} + \sum_{i\neq j}\epsilon_{ij}\left[\left(\frac{R_{o,ij}}{r_{ij}}\right)^{12} - 2\left(\frac{R_{o,ij}}{r_{ij}}\right)^{6}\right] + k_{ij}(r_{ij} - r_o)^2 \quad (5)$$

where $R_{o,ij} = {}^1/_2(R_{o,i} + R_{o,j})$ and $\epsilon_{ij} = (\epsilon_i\epsilon_j)^{1/2}$.

The force field parameters for Al, Si, O, and H were chosen to be the same as the reported CLAYFF parameters. We optimized the LJ parameters (*i.e.*, ϵ and σ) for Ge using the General Utility Lattice Program (GULP),[43] which employs nonlinear least-squares and energy minimization to fit the force field predictions to the experimental crystal structures of the three materials used. Initially, the C-phase of Na{$AlGeO_4$} (monoclinic space group $P2_1/n$ and lattice parameters a = 8.783 Å, b = 15.432 Å, c = 8.252 Å, α = β = 90°, γ = 90.09°) was used to derive the tetrahedral Ge−O LJ interaction parameters. The LJ values for the oxygen atoms were kept the same as the CLAYFF values, in accordance with the procedures used for development of that force field, whereas the tetrahedral Al LJ parameters were optimized to reproduce the observed Al−O bond distances. The tetrahedral Al parameters given in CLAYFF were developed for Al−O−Si linkages and could not reproduce the ideal Al−O bond lengths in Al−O−Ge linkages. The partial charges for Ge and Al were assigned to be the same as those for the tetrahedral Si and octahedral Al atoms, respectively, consistent with the parameter assignment procedure followed in CLAYFF to handle atoms in the same group of the periodic table. The initial Ge−O and Al−O interaction parameters were further refined by including the crystal structures of α-GeO_2 (hexagonal space group $P3_121$ and lattice parameters a = 4.9845 Å, b = 4.9845 Å, c = 5.6477 Å, α = β = 90°, γ = 120°) and the D-phase of K{$AlGeO_4$} (hexagonal space group $P6_3$ and lattice parameters a = b = 18.429 Å, c = 8.599 Å, α = β = 90°, γ = 120°) in the fitting procedure. Table 1 shows the final list of parameters. A summary of the predicted and experimental structural properties of the geometry-optimized C-phase of Na{$AlGeO_4$}, D-phase of K{$AlGeO_4$}, and α-GeO_2 is presented in the Supporting Information. To further validate the applicability of the force field, we compared the measured infrared spectra of the AlSiGeOH nanotubes at various compositions with the corresponding simulated vibrational power spectra of the nanotubes (see Results and Discussion). The spectra were computed by a 4096-point fast Fourier transform of the VACF obtained from a 5 ps NVT-MD simulation with a time step of 0.25 fs and trajectory sampling at every time step.

Molecular Dynamics Simulations. Atomically detailed models of AlSiGeOH nanotubes were built with x = 0, 0.25, 0.5, 0.75, and 1. The number of Al atoms in the circumference (N) ranged between 14 and 50, corresponding to nanotube outer diameters of 1.5–4.1 nm. The models were built using locally developed

computer codes that construct the asymmetric units of the nanotubes, apply the cylindrical symmetry operations, and prepare the fractional coordinates of the nanotube atoms for input to the MD simulation. All the MD simulations were carried out using the Discover module of Materials Studio 3.2 molecular simulation (Accelrys, Inc.). For AlSiGeOH nanotubes with both Si and Ge present, the substitution of Si with Ge atoms was carried out systematically, proceeding along the circumference. For example, at $x = 0.5$, every alternate Si atom along the circumference was replaced with a Ge atom, and at $x = 0.75$, one in every four Si atoms was replaced by Ge. The latter model was then used to obtain the structure for $x = 0.25$ by "inverting" the Si and Ge atom locations. All simulations were performed on electrically neutral and isolated nanotubes to avoid any effects of intertube interactions. The *a* and *b* dimensions of the orthorhombic unit cell were maintained at 7 nm (at least) to avoid intertube interactions. To avoid system size effects and generate a statistically valid ensemble, we used a supercell composed of two unit cells along the nanotube axis, with a resulting *c*-axis dimension of 1.68 nm. Simulations done with only one unit cell produced essentially the same results, albeit with a larger statistical error. The nanotube structures were first subjected to energy minimizations with steepest descent and conjugate gradient algorithms until the maximum energy gradient at any atom was below 1 $kcal \cdot mol^{-1} \cdot Å^{-1}$. The unit cell parameters were also allowed to be optimized during this step. The normal-mode vibrational frequencies were then calculated, and the radial breathing mode (RBM) frequency—which is sensitive to the nanotube diameter—was distinctly identified *via* the normal-mode eigenvectors. The optimized structures were then subjected to equilibration NVT-MD simulations at 298 K with a 0.9 fs integration time step for up to 20 ps. The energy and temperature of the systems were found be equilibrated typically within 1–2 ps. Subsequently, 100 ps NVT-MD simulations were performed to calculate the ensemble average internal energy (potential + kinetic) of the nanotubes as a function of their diameters using five 15 or 20 ps blocks of data to obtain an average energy and error bar. A Berendsen thermostat with a decay constant of 0.1 ps was used to control the temperature, because it was found to be much more stable than the Nosé−Hoover thermostat. Specifically, it allowed us to maintain the average temperature at 298 ± 7 K, which could not be uniformly achieved using a Nosé−Hoover thermostat, even after considerable effort in selecting the heat bath coupling strength. The equations of motion under the Berendsen thermostat do not strictly maintain the canonical ensemble (NVT) trajectories. However, it has been shown that, with a decay constant of 0.1 ps or higher, the fluctuations in kinetic energy are comparable to fluctuations in the total energy of the system.[44] Moreover, we did not observe any drift of the total energy with time, indicating that the deviations from the NVT ensemble are negligible in this case. Hence, we use this thermostat consistently across all the simulations to provide physically realistic results.

Acknowledgment. We acknowledge support from the ACS Petroleum Research Fund (no. 44074-G10) and partial support from the National Science Foundation (CTS-NIRT no. 0403574). We thank Y. Hudiono for assistance with EDX data collection.

Supporting Information Available: Description of and results on Gaussian curve fitting to the FTIR spectra of AlSiGeOH nanotubes, comparison of structural properties from atomistic geometry optimization simulations with crystal structure data of C-phase of $Na\{AlGeO_4\}$, D-phase of $K\{AlGeO_4\}$, and α-GeO_2, and comparison of calculated and measured vibrational frequencies of the nanotubes. This material is available free of charge *via* the Internet at http://pubs.acs.org.

REFERENCES AND NOTES

1 Allaoui, A.; Bai, S.; Cheng, H. M.; Bai, J. B. Mechanical and Electrical Properties of a MWNT/Epoxy Composite. *Compos. Sci. Technol.* **2002**, *62*, 1993–1998.
2 Avouris, P. Carbon Nanotube Electronics. *Chem. Phys.* **2002**, *281*, 429–445.
3 Balasubramanian, K.; Burghard, M. Biosensors Based on Carbon Nanotubes. *Anal Bioanal. Chem.* **2006**, *385*, 452–468.
4 Baughman, R. H.; Zakhidov, A. A.; de Heer, W. A. Carbon Nanotubes—The Route toward Applications. *Science* **2002**, *297*, 787–792.
5 de Heer, W. A.; Chatelain, A.; Ugarte, D. A Carbon Nanotube Field-Emission Electron Source. *Science* **1995**, *270*, 1179–1180.
6 Dresselhaus, M. S.; Dai, H. Carbon Nanotubes: Continued Innovations and Challenges. *MRS Bull.* **2004**, *29*, 237–239.
7 Martel, R.; Schmidt, T.; Shea, H. R.; Hertel, T.; Avouris, P. Single- and Multi-Wall Carbon Nanotube Field-Effect Transistors. *Appl. Phys. Lett.* **1998**, *73*, 2447–2449.
8 Niu, C. M.; Sichel, E. K.; Hoch, R.; Moy, D.; Tennent, H. High Power Electrochemical Capacitors Based on Carbon Nanotube Electrodes. *Appl. Phys. Lett.* **1997**, *70*, 1480–1482.
9 Zuttel, A.; Sudan, P.; Mauron, P.; Kiyobayashi, T.; Emmenegger, C.; Schlapbach, L. Hydrogen Storage in Carbon Nanostructures. *Int. J. Hydrogen Energy* **2002**, *27*, 203–212.
10 Klinke, C.; Bonard, J. M.; Kern, K. Thermodynamic Calculations on the Catalytic Growth of Multiwall Carbon Nanotubes. *Phys. Rev. B* **2005**, *71*, 035403(17) .
11 Robertson, D. H.; Brenner, D. W.; Mintmire, J. W. Energetics of Nanoscale Graphitic Tubules. *Phys. Rev. B* **1992**, *45*, 12592–12595.
12 Terrones, H.; Terrones, M. Curved Nanostructured Materials. *New J. Phys.* **2003**, *5*, 126.
13 Ago, H.; Ohshima, S.; Tsukuagoshi, K.; Tsuji, M.; Yumura, M. Formation Mechanism of Carbon Nanotubes in the Gas-Phase Synthesis from Colloidal Solutions of Nanoparticles. *Curr. Appl. Phys.* **2005**, *5*, 128–132.
14 Tenne, R.; Rao, C. N. R. Inorganic Nanotubes. *Philos. Trans. R. Soc. London Ser. B—Math. Eng. Sci.* **2004**, *362*, 2099–2125.
15 Tenne, R. Inorganic Nanotubes and Fullerene-Like Nanoparticles. *Nat. Nanotechnol.* **2006**, *1*, 103–111.
16 Pauling, L. The Structure of the Chlorites. *Proc. Natl. Acad. Sci. U.S.A.* **1930**, *16*, 578–582.
17 Mukherjee, S.; Kim, K.; Nair, S. Short, Highly Ordered, Single-Walled Mixed-Oxide Nanotubes Assemble from Amorphous Nanoparticles. *J. Am. Chem. Soc.* **2007**, *129*, 6820–6826.
18 Mukherjee, S.; Bartlow, V. A.; Nair, S. Phenomenology of the Growth of Single-Walled Aluminosilicate and Aluminogermanate Nanotubes of Precise Dimensions. *Chem. Mater.* **2005**, *17*, 4900–4909.
19 Farmer, V. C.; Adams, M. J.; Fraser, A. R.; Palmieri, F. Synthetic Imogolite—Properties, Synthesis, and Possible Applications. *Clay Miner.* **1983**, *18*, 459–472.
20 Konduri, S.; Mukherjee, S.; Nair, S. Strain Energy Minimum and Vibrational Properties of Single-Walled Aluminosilicate Nanotubes. *Phys. Rev. B* **2006**, *74*, 033401(14) .
21 Tamura, K.; Kawamura, K. Molecular Dynamics Modeling of Tubular Aluminum Silicate: Imogolite. *J. Phys. Chem. B* **2002**, *106*, 271–278.
22 Balevicius, V.; Fuess, H. Ion Induced Hypercritical Point in Tetrahydrofuran/Water Solutions. *Chem. Phys. Lett.* **2003**, *377*, 530–536.
23 MacDonald, S. A.; Schardt, C. R.; Masiello, D. J.; Simmons, J. H. Dispersion Analysis of FTIR Reflection Measurements in Silicate Glasses. *J. Non-Cryst. Solids* **2000**, *275*, 72–82.
24 Meneses, D. D.; Malki, M.; Echegut, P. Structure and Lattice Dynamics of Binary Lead Silicate Glasses Investigated By Infrared Spectroscopy. *J. Non-Cryst. Solids* **2006**, *352*, 769–776.
25 Cygan, R. T.; Liang, J. J.; Kalinichev, A. G. Molecular Models of Hydroxide, Oxyhydroxide, and Clay Phases and the Development of a General Force Field. *J. Phys. Chem. B* **2004**, *108*, 1255–1266.

26 Sandomirsky, P. A.; Meshalkin, S. S.; Rozhdestvenskaya, I. V.; Demyanets, L. N.; Uvarova, T. G. Crystal Structure of D-Phase of $K(AlGeO_4)$ and C-Phase of $Na(AlGeO_4)$. *Kristallografiya* **1986**, *31*, 883–891.

27 Smith, G. S.; Isaacs, P. B. Crystal Structure of Quartz-Like GeO_2. *Acta Crystallogr.* **1964**, *17*, 842–846.

28 Wada, S.; Wada, K. Effects of Substitution of Germanium for Silicon in Imogolite. *Clays Clay Miner.* **1982**, *30*, 123–128.

29 Bougeard, D.; Smirnov, K. S.; Geidel, E. Vibrational Spectra and Structure of Kaolinite: A Computer Simulation Study. *J. Phys. Chem. B* **2000**, *104*, 9210–9217.

30 Heinz, H.; Koerner, H.; Anderson, K. L.; Vaia, R. A.; Farmer, B. L. Force Field For Mica-Type Silicates and Dynamics of Octadecylammonium Chains Grafted To Montmorillonite. *Chem. Mater.* **2005**, *17*, 5658–5669.

31 de Boer, K.; Jansen, A. P. J.; Van Santen, R. A. Ab-Initio Approach to the Development of Interatomic Potentials for the Shell-Model of Silica Polymorphs. *Chem. Phys. Lett.* **1994**, *223*, 46–53.

32 Thorpe, M. F.; Galeener, F. L. Network Dynamics. *Phys. Rev. B* **1980**, *22*, 3078–3092.

33 Galeener, F. L. Band Limits and the Vibrational-Spectra of Tetrahedral Glasses. *Phys. Rev. B* **1979**, *19*, 4292–4297.

34 Pauling, L. The Structure of Some Sodium and Calcium Aluminosilicates. *Proc. Natl. Acad. Sci. U.S.A.* **1930**, *16*, 453–459.

35 Tripathi, A.; Parise, J. B. Hydrothermal Synthesis and Structural Characterization of the Aluminogermanate Analogues of JBW, Montesommaite, Analcime And Paracelsian. *Microporous Mesoporous Mater.* **2002**, *52*, 65–78.

36 Bursill, L. A.; Peng, J. L.; Bourgeois, L. N. Imogolite: An Aluminosilicate Nanotube Material. *Philos. Mag. A—Phys. Condens. Matter Struct. Defect Mech. Prop.* **2000**, *80*, 105–117.

37 Almairac, R.; Cambedouzou, J.; Rols, S.; Sauvajol, J. L. Diffraction of Oriented Nano-Peapods. *Eur. Phys. J. B* **2006**, *49*, 147–155.

38 Kadowaki, H.; Nishiyama, A.; Matsuda, K.; Maniwa, Y.; Suzuki, S.; Achiba, Y.; Kataura, H. Rietveld Analysis and Maximum Entropy Method of Powder Diffraction for Bundles of Single-Walled Carbon Nanotubes. *J. Phys. Soc. Jpn.* **2005**, *74*, 2990–2995.

39 Cambedouzou, J.; Pichot, V.; Rols, S.; Launois, P.; Petit, P.; Klement, R.; Kataura, H.; Almairac, R. On the Diffraction Pattern of C-60 Peapods. *Eur. Phys. J. B* **2004**, *42*, 31–45.

40 Rols, S.; Almairac, R.; Henrard, L.; Anglaret, E.; Sauvajol, J. L. Diffraction By Finite-Size Crystalline Bundles of Single Wall Nanotubes. *Eur. Phys. J. B* **1999**, *10*, 263–270.

41 Wada, K.; Yoshinaga, N. Structure of Imogolite. *Am. Mineral.* **1969**, *54*, 50–71.

42 Wada, S. I.; Eto, A.; Wada, K. Synthetic Allophane and Imogolite. *J. Soil Sci.* **1979**, *30*, 347–355.

43 Gale, J. D. GULP: A Computer Program for the Symmetry-Adapted Simulation of Solids. *J. Chem. Soc., Faraday Trans.* **1997**, *93*, 629–637.

44 Berendsen, H. J. C.; Postma, J. P. M.; Vangunsteren, W. F.; Dinola, A.; Haak, J. R. Molecular Dynamics with Coupling to an External Bath. *J. Chem. Phys.* **1984**, *81*, 3684–3690.